Efficient entrapment and separation of anionic pollutants from aqueous solutions by sequential combination of cellulose nanofibrils and halloysite nanotubes

Tuula Selkälä, Terhi Suopajärvi, Juho Antti Sirviö, Tero Luukkonen, Paivo Kinnunen, Kirsten I. Kling, Jakob B. Wagner, Henrikki Liimatainen

PII: S1385-8947(19)31266-5
DOI: https://doi.org/10.1016/j.cej.2019.06.008
Reference: CEJ 21880

To appear in: *Chemical Engineering Journal*

Received Date: 21 March 2019
Revised Date: 17 May 2019
Accepted Date: 2 June 2019

Please cite this article as: T. Selkälä, T. Suopajärvi, J.A. Sirviö, T. Luukkonen, P. Kinnunen, K.I. Kling, J.B. Wagner, H. Liimatainen, Efficient entrapment and separation of anionic pollutants from aqueous solutions by sequential combination of cellulose nanofibrils and halloysite nanotubes, *Chemical Engineering Journal* (2019), doi: https://doi.org/10.1016/j.cej.2019.06.008

Efficient entrapment and separation of anionic pollutants from aqueous solutions by sequential combination of cellulose nanofibrils and halloysite nanotubes

Tuula Selkälä[a], Terhi Suopajärvi[a], Juho Antti Sirviö[a], Tero Luukkonen[a], Paivo Kinnunen[a], Kirsten I. Kling[b], Jakob B. Wagner[b], Henrikki Liimatainen[a,*]

[a]*Fiber and Particle Engineering Research Unit, University of Oulu, P. O. Box 4300, FI-90014 Oulu, Finland*

[b]*Technical University of Denmark, DTU Nanolab, Fysikvej, Building 307, 2800 Kgs. Lyngby, Denmark*

**Corresponding author:* Tel: +358505659711. Email: henrikki.liimatainen@oulu.fi

Abstract

The synergistic combination of different nanomaterials for improved performance in environmental applications such as the removal of aqueous micropollutants has attracted increasing interest in recent years. This study demonstrates a novel sequential adsorption–aggregation concept that harnesses tubular halloysite nanotubes (HNTs) and flexible cellulose nanofibrils (CNFs) for the removal of a small, anionic dye molecule, chrome azurol S, from water. Hollow HNTs were first allowed to interact with the aqueous dye solution, after which the dye-loaded colloidal nanotubes were aggregated and separated from the water phase with cationized CNFs. The combination of 25 mg CNFs with 1 g HNTs at pH 7 resulted in efficient removal of dye (80%) and turbidity (~100%) and the removal of dye was further promoted in

more acidic conditions (within the pH range of 6–8.5) because of the attractive electrostatic interactions. Cationic CNFs not only enabled the separation of dye-loaded clay particles from the water phase through a rapid aggregation but also participated in dye removal through adsorption (~20%). In comparison with nano-sized HNTs, the dye removal performance of micro-sized and chemically similar kaolin was poor (43%). Given the good availability of both HNTs and CNFs and the low consumption of the more expensive component (i.e., CNFs) in the process, the concept is straightforward, readily applicable, environmentally benign, and potentially cost-effective.

Keywords: Deep eutectic solvent; Nanocellulose; Mordant blue 29; Nanoclay; Kaolin; Wastewater treatment

1 Introduction

Clays are naturally occurring inorganics, composed primarily of phyllosilicate minerals such as kaolinite and montmorillonite [1]. The atoms in phyllosilicates are arranged in tetrahedral and octahedral sheets that typically form layered and bulky platelets. Tubules, fibers, and laths of various sizes also exist [1]. Halloysite nanotubes (HNTs) are two-layered clay mineral particles with a chemical composition [$Al_2Si_2O_5(OH)_4 \cdot nH_2O$] similar to that of kaolinite [$Al_2Si_2O_5(OH)_4$] [2]. However, in contrast to platy kaolinite, HNTs typically have a hollow tubular morphology [2]. The tube walls of HNTs comprise ~15–20 aluminosilicate layers, with a spacing ranging from 1.0 nm (in hydrated form, $n = 2$) to 0.7 nm (in dehydrated form, $n = 0$) [3]. HNTs are polydisperse in size, typically having an outer diameter of 50–70 nm, lumen diameter of 10–20 nm, and length ranging from 0.5 to 1.5 μm [3]. The external surface and the inner lumen of

HNTs carry different charges at pH 2–8 in water [4], the former comprising negatively charged silica (SiO_2, ζ-potential ~ −50 mV) [5] and the latter comprising positively charged alumina (Al_2O_3, ζ-potential ~ +20 mV) [5]. The experimentally determined ζ-potential of HNTs in water at pH 4–8 is ~ −30 mV, which reflects the charge difference of these two layers [5]. Besides being abundant and inexpensive, HNTs have low *in vitro* [6] and *in vivo* [7] toxicity.

HNTs are versatile materials that can interact with and adsorb many different substances, thanks to the charge difference between the inner and outer surfaces. Driven by cationic electrostatic interactions, neutral and anionic substances can be loaded into the lumen of HNTs [3,8,9]. In addition, cationic substances can be adsorbed on the external surface of the tube [3,9]. Sometimes substances can even be intercalated between the layers of the tubes' walls [10]. Currently, HNTs are widely studied for biomedical purposes [11–13], but their potential for environmental applications has hitherto been underexplored. HNTs have been shown to adsorb e.g. anionic and cationic dyes [14–16], metal ions [17–19] and pharmaceuticals [20,21]. Therefore, one potential environmental application of HNTs is the treatment of various kinds of polluted waters [22,23]. The separation of nano-sized clay particles from water after the treatment and the hindered water flux in the packed column structures is often a challenge [24], although approaches, such as magnetic HNT adsorbents [25–27], have emerged.

To overcome these drawbacks, HNTs have often been combined with natural or synthetic polymers to form, for instance, beads [28–31], sponges [32] or membranes [33–37]. However, these methods typically require a significant amount of time and the use of additional chemicals. In a more straightforward approach, clay minerals have simply been mixed with a polymer to yield clay-polymer nanocomposites, which are then directly used for wastewater purification [38,39]. In another study, pristine HNTs were combined with a synthetic cationic polymer for the

removal of a cationic dye, basic blue 7, from water [24]. The mixing of HNTs with the polymer resulted in aggregation [40] and the formation of a HNT–polymer hybrid material, which was used as a matrix in column filtration of a dye solution. Although the hybrid was easily separated from water and transferred to a column, its dye removal performance was not optimum, as the cationic polymer covered the anionic surface of the HNTs, suggesting that better performance may be obtained if the HNTs are added to the treated mixture before the polymer is added.

Clays in general have been shown to adsorb, for instance, natural organic matter (NOM), thus converting it to an insoluble form, which can then be removed by coagulation–flocculation processes using a cationic polymer [41]. The polymer itself also participates in the purification process by partly adsorbing NOM and forming precipitates [41]. However, there is a lack of studies expanding this concept for the removal of dissolved molecules (e.g., micropollutants) from water, possibly because the conventional coagulation–flocculation treatment has previously been declared inefficient for simultaneous micropollutant removal [42]. In addition, new and effective bio-based materials are needed to replace older synthetic polymers. One promising candidate is cellulose nanofibrils (CNFs), which are elongated and flexible nanomaterials originating from, for example, the mechanical refining of wood pulp or a combination of chemical/enzymatic treatments and mechanical force [43]. Depending on the raw material and the production method, the width of CNFs is typically 5–60 nm, and the length is a few micrometers [44]. In addition, the CNFs be functionalized with e.g. anionic carboxylic groups [45–48] or cationic groups [49–55]. These functionalized CNFs can be designed using green solvent systems, such as recyclable deep eutectic solvents (DESs) [49].

In this study, we present a novel sequential approach that combines nanostructured clay and cellulose materials for the removal of small, anionically charged dye molecules from water.

HNTs were first loaded with dye molecules and then aggregated using CNFs to enable their efficient separation through sedimentation. CNFs also played a role in the removal of dye molecules through adsorption. The cationic CNFs were produced through sequential periodate oxidation and DES-mediated functionalization from cellulose and combined with HNTs for the enhanced removal of aqueous anionic dye chrome azurol S (CAS). Kaolin clay was used as a reference material in adsorption experiments. The effects of CNF dose, pH and mixing time on the dye and turbidity removal were investigated. The chemical characteristics, sizes, and morphologies of the HNTs, CNFs, and kaolin were analyzed using polyelectrolyte titration, diffuse reflectance infrared transform spectroscopy (DRIFT), wide-angle X-ray diffraction (WAXD), laser diffraction (LS), scanning electron microscopy (SEM), and transmission electron microscopy (TEM).

2 Materials and Methods

2.1 Raw materials and chemicals

Commercial softwood dissolving pulp (cellulose 96.2%, hemicelluloses 3.5%, total lignin <0.5%, acetone soluble extractives 0.17%; Domsjö Fabriker AB, Sweden) was used as the cellulose raw material. The dry sheets were disintegrated in deionized water before use. LiCl (Reag. Ph. Eur.; VWR, Belgium), sodium metaperiodate (<99.8%; Honeywell/Fluka, USA), glycerol (Reag. Ph. Eur.; VWR, Belgium), aminoguanidine hydrochloride (>98%; TCI, Japan), and ethanol (96%; VWR, France) were used in the synthesis of CNFs.

Halloysite nanotubes ($Al_2Si_2O_5(OH)_4 \cdot 2H_2O$; Aldrich, USA, product of Applied Minerals, Inc.), kaolin clay (Hydramatte®; KaMin LLC, USA), CAS (mordant blue 29, $C_{23}H_{13}Cl_2Na_3O_9S$, CAS number 1667-99-8; TCI, Japan), 0.1 M NaOH, and 0.1 M HCl (Oy FF-Chemicals Ab,

Finland) were used in the dye removal experiments. The properties of clays are presented in Table S1, and the structure and ionization scheme of CAS is given in Scheme 1. Buffer solutions with pH of 4, 7, and 10 (Oy FF-Chemicals Ab, Finland) were used for calibration of the pH meter.

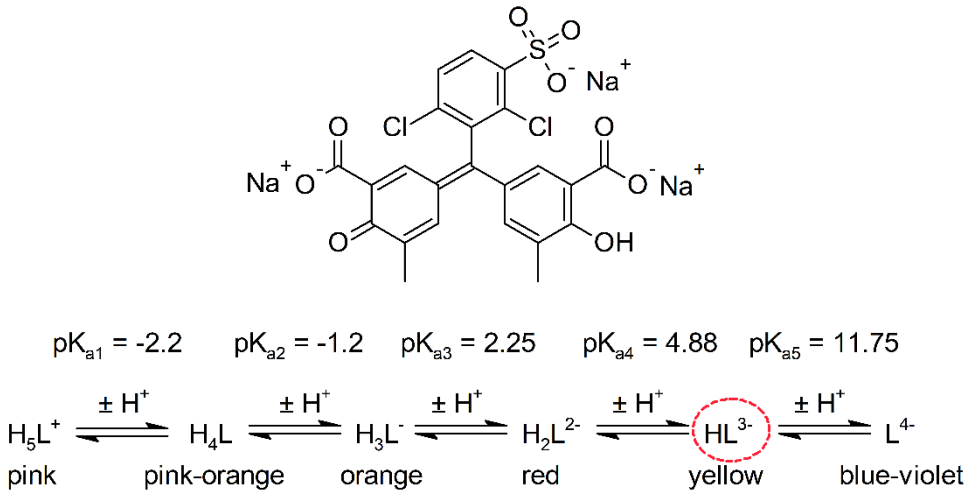

Scheme 1. The structure of chrome azurol S, its dissociation species, and the corresponding colors [56]. The highlighted species HL^{3-} corresponds to the presented chemical structure.

Commercial 0.5 M buffer solutions (citrate pH 3, sodium citrate pH 5, sodium phosphate pH 7, sodium phosphate pH 8, carbonate pH 9, and carbonate pH 10; Alfa Aesar, Germany) were used in the charge density measurements of the cationic CNFs. Anionic sodium polyethylene sulfonate (Pes-Na, 0.001 N; BTG Instruments GmbH, Germany) was employed as the titrant.

All reagents were used as received. Deionized water was used throughout the experiments.

2.2 Cationization of cellulose and disintegration into nanofibrils

Cationized dialdehyde cellulose (CDAC) was synthetized according to a previously reported two-step procedure (Scheme 2) [49]. First, dialdehyde cellulose (DAC) was synthetized through regioselective oxidation, in which the vicinal hydroxyl groups are oxidized to aldehyde groups using sodium metaperiodate. LiCl improves the oxidation efficiency by disrupting the hydrogen bond network of cellulose and thereby making more hydroxyl groups available to periodate [57]. Then, DAC was cationized in aminoguanidine hydrochloride–glycerol (AhG) DES, which acted as both a reaction medium and a reagent (aminoguanidine hydrochloride).

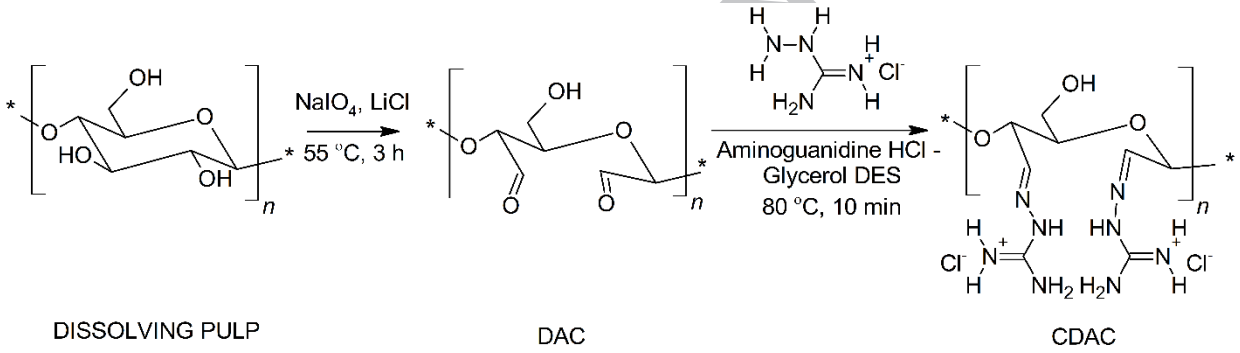

Scheme 2. Cationization of cellulose pulp via periodate oxidation, followed by imination in aminoguanidine hydrochloride-glycerol deep eutectic solvent.

To synthetize DAC, 1% (w/w) dissolving cellulose pulp (10 g abs.) in deionized water was reacted with LiCl (18 g) and sodium metaperiodate (8.2 g) for 3 h at 55 °C. Ethanol (500 mL) was added to stop the reaction, after which the resulting mixture was filtered. The collected DAC was first washed with 50:50 ethanol:water solution (500 mL), then mixed with ethanol (500 mL) for 30 min, filtered, and finally washed with ethanol (250 mL).

The AhG DES used for the synthesis of CDAC was prepared by heating and mixing aminoguanidine hydrochloride (75 g) and glycerol (125 g) in a beaker at 90 °C in an oil bath

until a clear liquid was formed. The temperature was adjusted to 80 °C, DAC (10 g abs.) was added, and the mixture was effectively mixed for 10 min. The beaker was then removed from the oil bath and ethanol (250 mL) was added, under stirring, to the mixture. The mixture was filtered and the collected CDAC was thoroughly washed with ethanol (950 mL). Finally, CDAC was mixed with deionized water (400 mL) for 10 min and collected by filtration.

Cationic CNFs were produced from CDAC by mechanical disintegration using a microfluidizer (Microfluidics M-110EH-30, USA). A 1% (w/w) CDAC dispersion in water was passed twice through 400 and 200 μm chambers at a pressure of 1000 bar. The dry content of the resulting CNF suspension was determined by drying two samples at 105 °C overnight and taking the average of the two results. The result was 1% (w/w).

2.3 Characterization

2.3.1 Characterization of charge density of CNFs by polyelectrolyte titration

Buffer stock solutions (0.5 M) in the pH range 3–10 were diluted to 0.5 mM with deionized water and the pH was adjusted, when necessary, with 0.1 M NaOH/HCl. The 1% (w/w) CNF suspension was diluted with deionized water to 0.1% (w/w). The samples for charge density determination were prepared by mixing 1 mL CNF suspension and 9 mL buffer solution in the sample cell of the particle charge detector (Mütek PCD 03, USA), after which the mixture was titrated with Pes-Na. The measurement was repeated three times at each buffer solution (pH 3, 5, 7, 8, 9, 10). The stability of the charge over time was investigated by repeating the measurement four times at one-month intervals.

2.3.2 Characterization of cellulose structure by diffuse reflectance infrared Fourier transform spectroscopy

DRIFT spectra of oven- or freeze-dried cellulose samples (pulp, DAC, CDAC, CNFs) were recorded in the wavelength 800–4000 cm^{-1}, using 40 scans with a resolution of 4 cm^{-1} (Bruker Vertex 80V, USA).

2.3.3 Characterization of cellulose crystallinity by X-ray diffraction

The crystalline structures of pristine cellulose pulp, DAC, CDAC, and CNFs were analyzed by wide-angle X-ray diffraction, using a Rigaku SmartLab 9 kW rotating-anode diffractometer (Japan) equipped with a Cu Kα radiation source (λ = 0.1542 nm, 45 kV, 200 mA). Scans were taken over a 2θ (Bragg angle) range of 4–45° at a scanning speed of 1.5°/min and a step size of 0.05°. The degree of crystallinity (CrI) was calculated based on the peak intensity of the crystalline plane (I_{200}) located at 22.5° and the peak intensity at 18.5° associated with the amorphous fraction of cellulose (I_{am}). CrI values were calculated using the Segal method [58] (Equation 1):

$$CrI = [(I_{200} - I_{am})/I_{200}] \times 100\% \quad (1)$$

2.3.4 Characterization of kaolin clay particle size by laser diffraction

The particle size of kaolin clay was measured using a Beckman Coulter LS 13 320 particle size analyzer (USA). Slurry with a dry matter content of 0.2% (w/v) was prepared by the addition of dry powder to water. The slurry was ultrasonicated (37 kHz, pulse mode, 100% power), combined with overhead mixing, for 15 min before measurement.

2.3.5 Characterization of morphology, structure, and size of HNTs and CNF and morphology of kaolin clay by TEM

Samples were prepared for TEM analyses by drop-casting diluted HNT, kaolin, and CNF suspensions onto Cu-TEM grids with lacey carbon film and allowing them to dry before insertion into the microscope. HNT samples were prepared from solution by diluting 1 droplet (~5 µL) in 1.5 mL ethanol twice. A spatula tip of kaolin powder was dispersed in 1.5 mL ethanol. The samples were sonicated for 3 min and ~5–10 µL of each sample was pipetted onto a TEM grid. HNT and kaolin samples were investigated in a TECNAI T20 G2 TEM (FEI Company, USA), equipped with a US1000 CCD camera (Gatan, Inc., USA), at 200 kV. The water-dispersed CNF sample was analyzed in an image-corrected (Cs corrected) FEI TITAN ETEM equipped with a monochromator and a Gatan OneView camera, operated at 80 kV.

The HNT diameter and lumen width distributions were obtained by measuring $n > 100$ individual HNTs using ImageJ/FIJI software (National Institutes of Health, USA). Gaussian fitting was employed to evaluate the peak centers (OriginPro 2018 software; Origin-Lab Corporation, USA).

2.3.6 Characterization of CAS-loaded HNT/kaolin-CNF aggregate morphology by cryo-SEM

Cryo-scanning electron microscopy (Quanta 200 FEG ESEM, equipped with Quorum cryo transfer system and stage) was used to characterize the morphology of CAS-loaded HNT/kaolin-CNF aggregates (CAS 50 mg/L, HNT or kaolin 2 g/L, CNFs 10 mg/g). The aqueous aggregates were dipped into slushed liquid N_2, fractured in the prep chamber, and transferred to the SEM

chamber (−190 °C) for pre-imaging. After 1 h sublimation (−70 °C), the sample was coated (8 s) with Pt and transferred back to the SEM chamber for imaging (−190 °C) at 12 kV.

2.4 Removal of CAS from water by a sequential combination of HNT/kaolin and CNFs

All experiments followed a similar procedure, wherein CAS was first allowed to interact with and adsorb to HNTs or kaolin, after which CNFs were added to enable the aggregation and separation of CAS-loaded HNTs/kaolin via sedimentation (Scheme S1). The effects of CNF dose, pH and mixing time on dye removal were examined. In addition, the removal of colloidal particles by CNFs was monitored by measuring the turbidity of the treated samples (except in the mixing time experiments). The concentrations of the clay mineral and CAS were kept constant at 2 g/L and 50 mg/L, respectively. The experiments concerning the effect of CNF dose and pH on CAS and turbidity removal were performed in triplicate, and sample standard errors were calculated. The experiments were conducted in non-buffered conditions at room temperature, using 150 mL beakers equipped with magnetic stirring bars. An aqueous CAS stock solution (1000 mg/L) was prepared and stored at room temperature. The same stock solution was used for all experiments. The CNF suspension was diluted to 0.2% (w/w) (~2000 mg/L) with deionized water immediately before use.

In a typical experiment, HNTs or kaolin (0.2 g, equal to 2 g/L) was weighed on a beaker and deionized water (92.5–95 mL) was added. Then, the mixture was ultrasonicated for 15 min to facilitate the wetting and dispersion of the clay mineral. CAS stock solution (5 mL, equal to 50 mg/L) was then added, and the pH of the mixture was adjusted to the desired value (6–8.5) by adding a few microliters of 0.1 M NaOH or HCl. The mixture was stirred at 200 rpm for 24 h, CNF solution (0–2.5 mL, equal to 0–50 mg CNFs/g clay) was added to reach the final volume

(100 mL), and stirring at 200 rpm was continued for another 24 h. The mixture was allowed to settle for 30 min, after which aliquots (4×10 mL) were pipetted from the center of the mixture (2 cm from the bottom of the beaker), and the turbidity of each sample was measured (Hach Ratio XR turbidimeter model 43900, USA). Then, the sample was centrifuged (Beckman Coulter Avanti J-26 XPI, USA) at 6500 rpm for 20 min at 5 °C, and the supernatant was collected. Finally, the pH of the supernatant was recorded.

The impact of mixing time on CAS removal was studied separately for HNTs and CNFs. Mixing time with HNTs was 0–24 h. In the case of CNFs, HNTs were first allowed to interact with CAS for 24 h, after which CNFs were added to the mixture and the mixing was started. Mixing time was 1 min–24 h. In both cases, the 30 min sedimentation and turbidity measurement were excluded.

Experiments involving the use of premixed HNT–CNF hybrid as adsorbent were also performed (referred to as 1–step method). The hybrid was formed by mixing HNTs (0.2 g) with CNFs (1.5 mL, equal to 15 mg/g HNTs) for 20 s using a vortex mixer, after which the mixture was sedimented for 20 min. The hybrid was poured to the CAS solution (50 mg/L, pH 7) and the mixture was stirred either for 3 min or 24 h at 200 rpm. 30 min sedimentation was excluded for the sample mixed for 3 min but included for the sample mixed for 24 h (for comparison purposes).

The concentration of CAS in the supernatant was analyzed by ultraviolet-visible (UV-vis) spectroscopy (Shimadzu UV-1800, Japan) at 427 nm using quartz cuvettes. In addition, the spectrum at 200–800 nm was recorded for each sample to detect any changes in the location of the absorbance maximum. The baseline correction was performed using a blank sample, which contained only clay (2 g/L HNTs or kaolin) and had the same pH as the actual sample. These

blank samples were prepared at the same time and treated in the same manner as the actual samples, as described earlier. Experiments were also conducted without HNTs or kaolin to study the effect of CNFs (30 mg/L) alone on CAS removal at pH 6–8.5. The sample preparation, sampling, and analysis were identical to those described above, with the exception of the turbidity measurements. For these samples, the baseline correction was performed using deionized water. For all samples, the percentage of removed CAS from the mixture was calculated using Equation 2:

$$\% \text{ CAS removed} = [(C_0 - C_e)/C_0] \times 100 \quad (2)$$

where C_0 (mg/L) and C_e (mg/L) are the initial and the equilibrium concentrations of CAS, respectively. The spectrophotometer was calibrated for the CAS concentration range 0–60 mg/L at pH 7, using deionized water as a reference (Figure S2). In addition, the impact of the solution pH (6–8) on the calibration was studied, and it proved to be insignificant. The accuracy and daily variation of the method, as well as the stability of the CAS, were monitored by measuring CAS solutions of known concentration (10 and 40 mg/L, pH 7) throughout the course of the study.

The performance of the turbidimeter was monitored by measuring Gelex® Secondary Turbidity Standards (0.042, 1.49, 16.6, 158, and 1743 NTU) before actual samples were measured. The removed turbidity was calculated by comparing the readings of an actual sample (NTU_S) and a reference sample (NTU_R, otherwise identical but did not contain any CNFs) (Equation 3):

$$\% \text{ turbidity removed} = [(NTU_R - NTU_s)/NTU_R] \times 100 \quad (3)$$

To ensure that CNFs alone did not have a significant impact on the UV-vis spectra or the turbidity results, solutions with CNF concentrations of 5–100 mg/L at pH 7 were prepared and analyzed. The samples were prepared by diluting 1% CNF suspension to the desired concentration with deionized water and adjusting the pH to 7 with 0.1 M HCl/NaOH. The solution was mixed for 40 min at 200 rpm, after which it was allowed to settle for 30 min. The sampling and analysis were identical to those described earlier. The results showed that CNFs did not absorb at wavelengths >400 nm, and the impact on turbidity was negligible (Figure S3, Table S2).

The amount of adsorbed CAS per unit mass of adsorbent (HNTs/kaolin, CNFs or combination of HNTs/kaolin and CNFs) at time t, q_t (mg/g) and at equilibrium, q_e (mg/g), were calculated using Equations 4 and 5, respectively:

$$q_t = [(C_0 - C_t)/m] \times V \quad (4)$$

$$q_e = [(C_0 - C_e)/m] \times V \quad (5)$$

where C_0 (mg/L), C_t (mg/L) and C_e (mg/L) are the initial concentration, concentration at time t (min) and concentration at equilibrium of CAS, respectively. V is the volume of the solution (L) and m is the dry weight of adsorbent (g).

3 Results and Discussion

3.1 Effect of CNF dose on the combined dye removal process

A significant difference was observed between HNTs and kaolin in CAS removal at pH 7 (Figure 1). Combining 25 mg CNFs with 1 g HNTs (i.e., CNF dose 25 mg/g) resulted in maximum CAS removal of 80% (q_e 19 mg/g), whereas with kaolin only 43% (q_e 11 mg/g) removal was achieved. Interestingly, HNTs alone removed 42% of CAS (q_e 10 mg/g), but kaolin alone removed only 7% of CAS (q_e 2 mg/g). As the CNF dose increased from 2.5 to 25 mg/g, the trend of removal was almost linear, indicating that complete removal of CAS may be possible. Indeed, a nearly complete removal of CAS (97% and 89% with HNTs and kaolin, respectively) was achieved when the CNF dose was increased to 50 mg/g (Figure S4). However, overdosing resulted in incomplete removal of CNFs and restabilization of HNTs via a charge reversal [59], which manifested as a hazy mixture and floating aggregates (Figure S5). An additional filtration step (0.2 μm syringe filter) was required to eliminate interference during analysis; therefore, these conditions were not studied further. The observed improvement in the removal of CAS as a function of CNF dose was probably an outcome of the increased portion of CAS adsorbed onto CNFs, as the adsorption capacities of clay minerals are assumed to remain constant (the concentration of clay minerals and CAS, stirring time, and speed were constant). This dye fraction adsorbed on CNF was then removed from the solution together with the aggregates. Based on these results, it can be deduced that CNFs play a dual role in the studied process: they promote destabilization and aggregation of the colloidal clay mineral particles and they adsorb CAS. These findings are in line with previous results that cationic CNFs are efficient kaolin aggregators [59,60] and that functionalized CNFs work as efficient adsorbents for charged molecules [61].

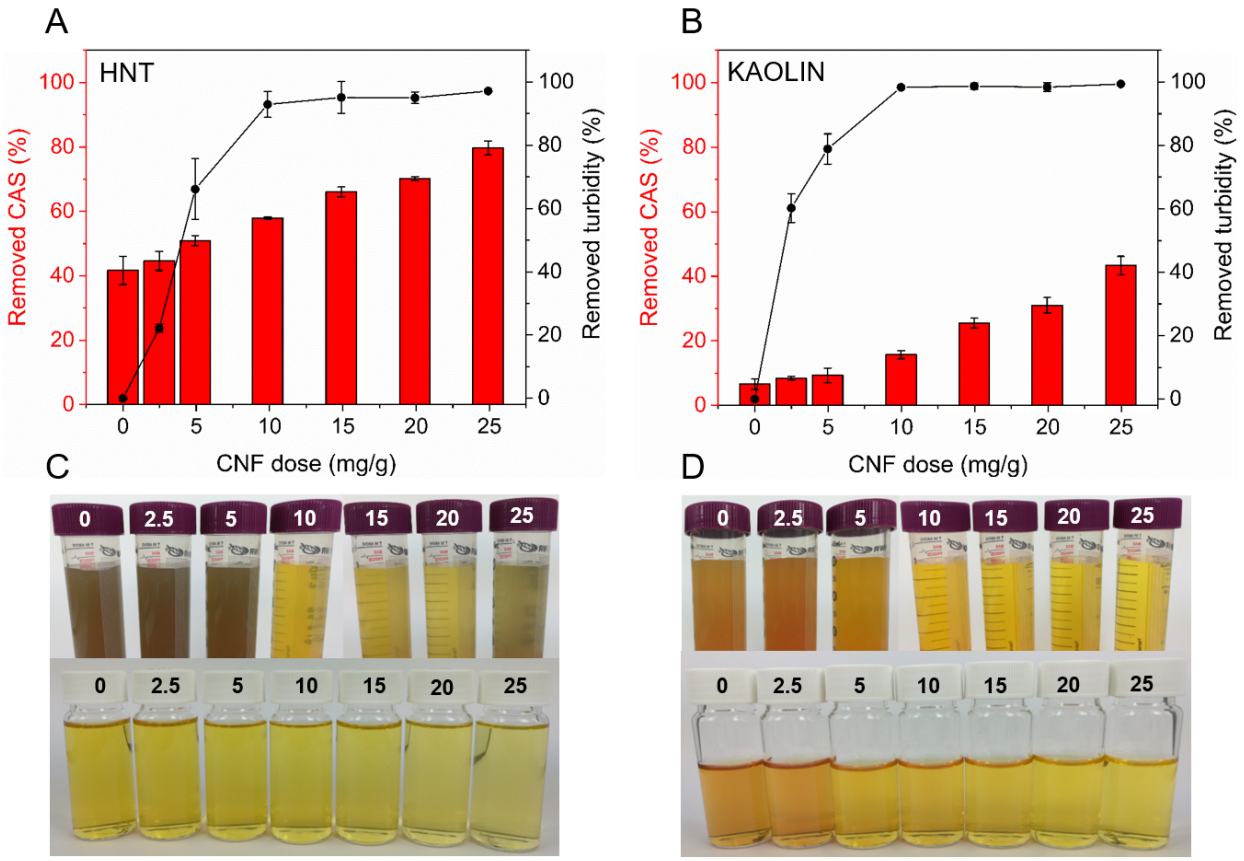

Figure 1. Amount of chrome azurol S (%, bars) and turbidity (%, lines) removed as a function of the cellulose nanofibril dose using (A) halloysite nanotubes and (B) kaolin at pH 7. The data points are averages of three repetitions and the error bars represent the sample standard deviation. Photographs of the samples that were employed for turbidity measurements (top) and the same samples after centrifugation (bottom) using (C) halloysite nanotubes and (D) kaolin. The numbers on the photographs refer to the cellulose nanofibril dose (0–25 mg/g).

The addition of CNFs decreased the turbidity of the samples (Figure 1), indicating efficient aggregation and sedimentation of CAS-loaded clay mineral particles. Irrespective of the clay mineral type, 10 mg/g of CNFs was enough to reach almost complete colloid removal. CAS-loaded HNTs and kaolin remained as stable colloidal particles in the solution when no CNFs were added to the mixture (0 mg/g, Figure S5), implying that CNFs are required to attain

efficient purification. Differences in the removal of turbidity were observed only with the lowest CNF doses (2.5–5 mg/g), where samples containing kaolin performed better. A possible explanation is that individual kaolin particles are larger than HNTs, which may result in faster sedimentation of kaolin–CNF aggregates compared to HNT–CNF aggregates. When the CNF dose was increased above 5 mg/g, the effect of particle size became insignificant.

The samples underwent peculiar color changes during the process (Figure 1C and D and Figures S5 and S6). With HNTs, the color of the mixture turned from orange to brown as the pH was adjusted from 5.2 to 7 and the mixture was stirred for 24 h. This color may be a result of two phenomena occurring in the system: First, CAS (HL^{3-} species, Scheme 1) diffused into the lumen of HNTs and formed a complex with aluminum (Al–OH), which is purple in color [62]. HNTs are transparent [5], enabling the color to show through. The remaining CAS molecules in the solution made the solution appear yellow at pH 7, whereas, as it mixed with the purple HNT–CAS complex, the outcome was brown (complementary colors). The mixture turned purple within 10 min as CNFs were added; the more CNFs were added, the more intense the purple color became. This was likely the outcome of decreasing CAS concentration (yellow color) with increasing CNF concentration. The sedimented HNT–CAS–CNF aggregates were purple.

With samples containing kaolin, the suspension remained orange but became slightly muted in tone as the pH was adjusted from 6.7 to 7 and the mixture was stirred for 24 h. This was an indication that CAS was binding to kaolin to some extent. Surprisingly, the mixture turned bright green within 10 min as CNFs were added. This was because the kaolin–CAS complex was not deep purple (as with HNTs) but light blue. As CNFs removed CAS, the yellow color of the solution becomes less intense, allowing the blue of the kaolin–CAS complex to show through, resulting in a green color. The sedimented kaolin–CAS–CNF aggregates were light blue to blue

in color. In addition, it should be noted that no color changes occurred when pure CNFs were mixed with pure CAS solution.

3.2 The role of CNFs in the combined dye removal process

The principal mechanism of aggregation of CAS-loaded HNTs or kaolin clay with cationic CNFs is likely to be charge neutralization, owing to the high charge density of the nanofibril surface [59,60]. The elongated cationic CNFs adsorbed and attached to the surface of anionic HNTs via electrostatic forces, resulting in charge neutralization, destabilization, and, eventually, sedimentation of the HNT–CAS–CNF aggregates (Scheme 3A). The destabilization of HNT suspension was not caused by the loading of CAS, because the loading of anionic substances inside HNTs is known to increase the negative ζ-potential and stabilize the dispersion [3,9]. The net surface charge of kaolin particles is negative at pH > 2 in water [63,64]. However, the individual platelets have a pH-dependent surface charge: The basal surfaces (faces) carry a permanent negative charge, while the pH-dependent edges are positively charged at pH < 7.2 [65], owing to the protonation of the edge aluminol group [64]. The utilization of the interlayer space between the platelets typically requires additional treatments such as methoxy-modification on the interlayer surface hydroxyl groups [66], because the platelets are large and held together by strong hydrogen bonds and the structure does not swell when wetted [67]. Therefore, the most prominent adsorption site for anionic CAS on kaolin is the edges (Scheme 3B). The lack of suitable adsorption sites partially explains the low CAS removal percentage (7%) obtained for kaolin without CNFs (in addition to lower surface area). As with HNTs, the addition of CNFs neutralized the surface charge of kaolin and resulted in sedimentation (Scheme 3B).

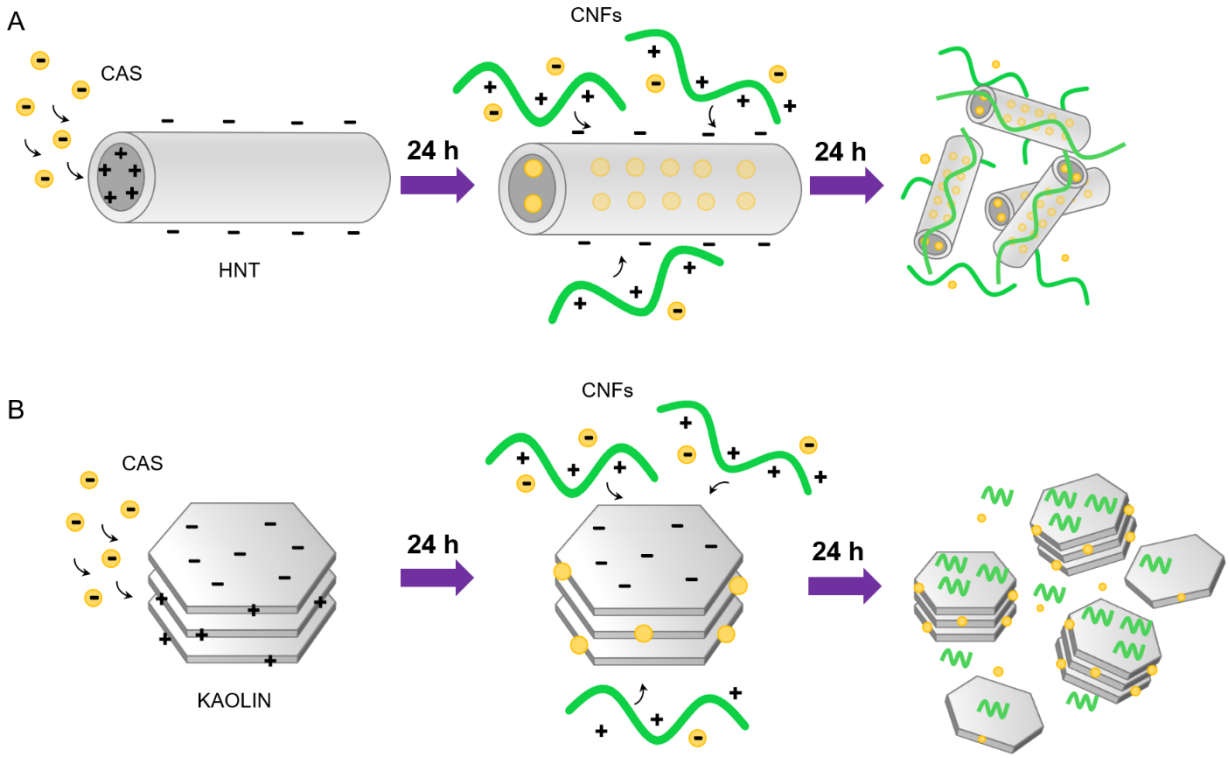

Scheme 3. Illustration of chrome azurol S removal and halloysite nanotube/kaolin aggregation mechanisms with (A) halloysite nanotubes and (B) kaolin clay.

3.3 Effect of pH on the combined dye removal process

The removal of CAS was more efficient under acidic conditions than under more basic conditions with both clay minerals (Table 1), as has been noted before [63]. The pH range of 6–8.5 was selected because it is a typical range for municipal wastewater treatment. When pH decreased from 8.5 to 6, the removal of CAS increased by ~40 percentage points with HNTs and by ~30 percentage points with kaolin. At all studied pH levels, the removal of CAS was more efficient with HNTs than with kaolin. At pH 6–8.5, the dominating CAS species is HL^{3-} as the pK_a of H_2L^{2-} is 4.88 (Scheme 1). The ζ–potentials of HNTs and kaolin are negative at pH 3–11 and the point of zero charges (pH_{pzc}) are 2.75 and 2.40 for HNTs and kaolin, respectively [63].

This indicates that the outer surfaces of HNTs and kaolin are anionic at pH 3–11. Moreover, the lumen of HNTs is cationic at pH 2–8 [63], which suggests that the anionic CAS species was able to electrostatically interact and adsorb to HNT lumen at the studied pH range of 6–8.5. The observed increase in the CAS removal in the more acidic region is likely to be an outcome of the fact that above pH 8, the lumen loses it positive charge [63]. Thus, the electrostatic interaction between the HNT lumen and the anionic CAS species decreases as the pH increases. In the case of kaolin, the edges of the platelets become positively charged at pH < 7.2 [65], which explains the slight increase in the CAS removal observed at pH ≤ 7.

Table 1. Removal of chrome azurol S and turbidity of the suspensions as a function of solution pH, using either halloysite nanotubes or kaolin clay, with or without cationic cellulose nanofibrils (15 mg/g)

pH	HNTs	Kaolin

	CAS removed (%)		Turbidity removed (%)	CAS removed (%)		Turbidity removed (%)
	No CNFs	**With CNFs**	**With CNFs**	**No CNFs**	**With CNFs**	**With CNFs**
6[a]	64 ± 2	84 ± 4	96.6 ± 0.9	29.7 ± 1.4	52 ± 8	98.6 ± 1.3
6.5[a]	48 ± 4	69 ± 6	96.5 ± 0.9	14 ± 4	33 ± 4	98.1 ± 1.4
7	42 ± 5	66 ± 2	95 ± 6	7 ± 2	25 ± 2	98.7 ± 1.0
7.5	32.4 ± 0.6	52 ± 3	94 ± 6	5 ± 2	18.7 ± 1.2	99.6 ± 0.3
8	29 ± 2	47 ± 4	96 ± 3	3 ± 2	19 ± 3	95 ± 4
8.5	23 ± 3	43 ± 2	95 ± 3	3 ± 3	17.4 ± 1.5	98 ± 2

[a] Additional signal observed in the UV-vis spectra.

The addition of CNFs (15 mg/g) to the HNT/kaolin–CAS mixture increased the CAS removal by ~20 percentage points with both clay minerals, emphasizing the benefit of combining these two materials (Table 1). In addition, the observed increase was not dependent on the pH, which was a consequence of the stable negative surface charge on both clays and the stable cationic charge on CNFs. Regarding the turbidity, ~90–100% removal was obtained through the whole pH range with both HNTs and kaolin (Table 1). Cationic CNFs have also shown a good adsorption capacity for anionic humic acid (310 mg/g at pH 6) [68]. Similarly to clays, humic acid naturally adsorbs waterborne pollutants (e.g., heavy metal ions, dyes), and it has been found that porous foams prepared from CNF–humic acid complexes efficiently remove cationic dyes (up to 55%) and copper(II) metal ions (30%) [68]. This confirms the notion that combinations of natural materials can be beneficial for pollutant removal.

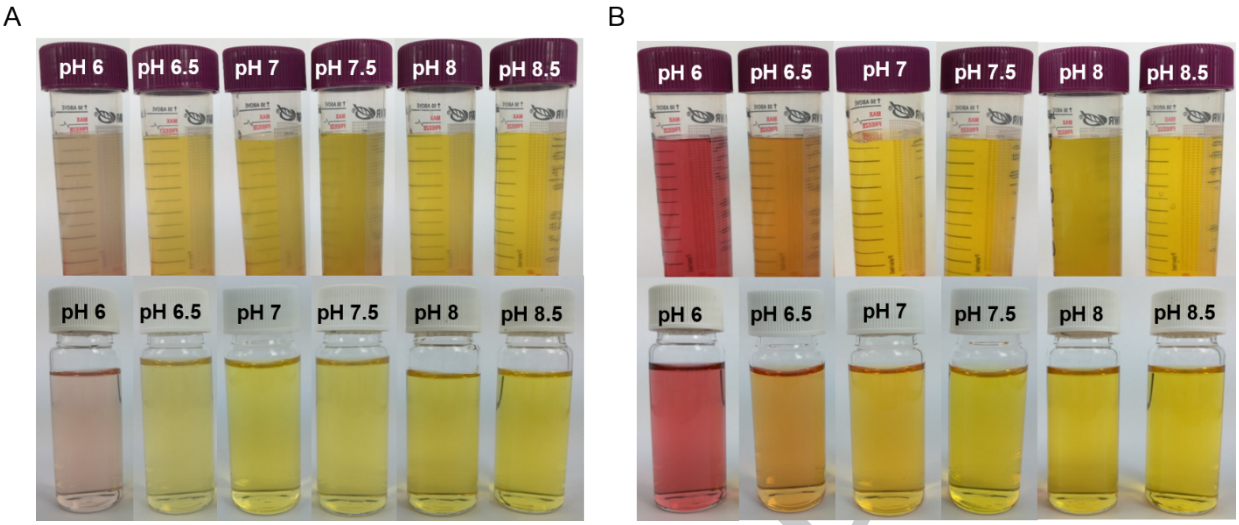

Figure 2. Photographs of the samples that were used for the turbidity measurements (top) and the same samples after centrifugation (bottom), using (A) halloysite nanotubes and (B) kaolin (cellulose nanofibril dose 15 mg/g, pH 6–8.5).

The impact of CNFs alone on CAS removal was verified by treating pure CAS solution with CNFs (15 mg/g, corresponding to 30 mg/L) at pH 6–8.5; the results showed consistent removal rates of 21–24% (q_e 348–405 mg/g) (Figure S7). Previously, we used anionic CNFs as an adsorbent for pharmaceutical salbutamol and obtained ~12% removal with 25 mg/L CNFs (q_e(exp) 196 mg/g) [61]. The higher removal efficiency observed in the current study compared with the previous one can be attributed to differences in the pollutant type and functional groups on CNFs, as well as their higher charge density.

The samples prepared at pH values of 6 and 6.5 (with and without CNFs) had an additional signal at the wavelength of 544–546 nm in the UV–vis spectra (Figure S8). The signal was more pronounced with kaolin than with HNTs. The samples at pH 6 also differed in color from the other samples (Figure 2). The additional signal at 544–546 nm was not present in the pure CAS

solution, in the pure clay mineral or CNF samples, or in the CAS–CNF samples. Therefore, it is likely attributable to electrostatic interaction or complex formation between CAS and clay mineral surfaces at those pH values, as has been noted previously between anionic azo dyes and HNTs [14]. Interestingly, highly acidic CAS solutions (dominating species H_5L^+, Scheme 1) [56] and CAS–aluminum complexes [69–71] have adsorption maxima at ~544–546 nm. Thus, it can be postulated that the supernatant samples contained residual CAS–clay colloidal particles at pH 6–6.5, and the complex formation between CAS and aluminum was sufficiently intense to become visible in the UV spectra. Based on the literature [71], aluminum–CAS complex does not adsorb at 427 nm, which was the peak used for the quantification of CAS in the current study. Therefore, the effect of the additional signal at 544–546 nm on the results presented in Table 1 can be considered negligible.

A summary of the adsorption capacities of HNTs, kaolin, CNFs, HNT–CNF and kaolin–CNFs, as well as their comparison to commonly used adsorbents in anionic dye removal is presented in Table S3.

3.4 Effect of mixing time on the dye removal and comparison of the addition methods

HNTs alone removed immediately 27% of CAS (Figure 3). However, a steady increase in the CAS removal was observed as the mixing time increased, as expected, since the process is diffusion-driven. 24 h was required to reach the 40% removal as seen in Figure 1 (CNF dose 0 mg/g), which indicated that the 24 h mixing is justified in the first step of the process. The adsorption capacity q_t of HNTs was 6.5–9.4 mg/g.

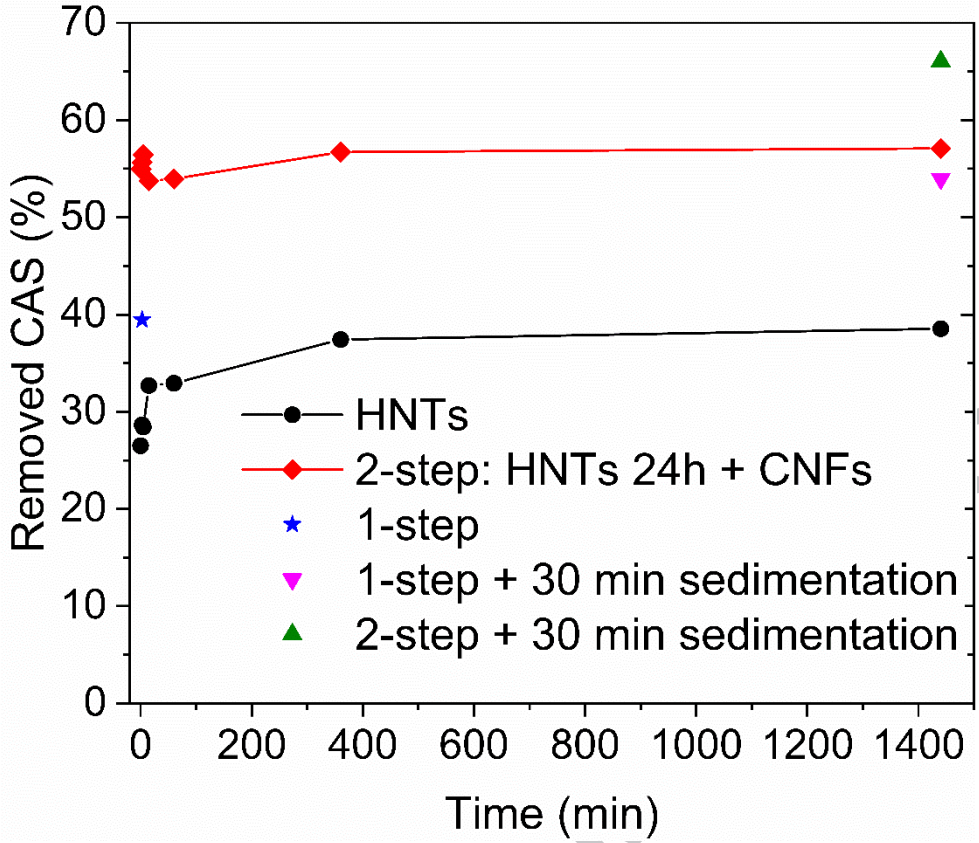

Figure 3. Removal of chrome azurol S as a function of mixing time. Spheres: Only halloysite nanotubes (HNTs), mixing time 0–24 h; Squares: HNTs followed by cellulose nanofibrils (CNFs), mixing time 1 min–24 h with CNFs; Asterisk: HNT–CNF hybrid, mixing time 3 min; Downward triangle: HNT–CNF hybrid, mixing time 24 h and additional 30 min sedimentation; Upward triangle: HNTs followed by CNFs, mixing time 24 h with CNFs and additional 30 min sedimentation.

In contrast to CAS adsorption on HNTs, the adsorption of CAS on CNFs was fast (Figure 3). There was no evident improvement in the CAS removal when the mixing time after CNFs addition was increased from 1 min to 24 h during the sequential, 2-step process (54–57%, q_t 13–14 mg/g). The result was not surprising, because it is known that the adsorption of organic

pollutants on CNFs is rapid [61]. Regarding the turbidity of the samples, an immediate floc formation and sedimentation was observed in the samples mixed for 1–60 min, and the supernatants were transparent (Figure S9). The samples mixed for a longer period (6–24 h) were initially more turbid, which implied that the flocs had partly been broken. The results indicate that the mixing time in the CNF addition step can be reduced to a few minutes, without having to compromise the dye removal efficiency or turbidity reduction. However, if longer mixing times are used, it is advisable to include a 30 min sedimentation period.

Experiments were also performed to demonstrate the differences of using the 2–step or 1–step addition method, i.e. simultaneous addition of both HNT and CNF to form a HNT–CNF hybrid as an adsorbent (Figures 3 and S9). It was observed, that 3 min mixing with HNT–CNF hybrid removed 39% (q_t 10 mg/g) of CAS, which was 10 percentage points better than with HNTs alone, but 17 percentage points less than with the 2-step method using 3 min mixing. The result was expected, because the time was too short for CAS molecules to diffuse inside the tubes. HNT–CNF hybrid mixed for 24 h followed by 30 min sedimentation removed 54% (q_t 13 mg/g) of CAS, whereas with the 2-step method combined with 30 min sedimentation the removal was 66% (q_t 16 mg/g). The poorer performance of the 1-step method compared with the 2-step method may be a result of the blockage of the tubes by CNFs (lumen diameter ~15 nm, CNF diameter <5 nm) during the preparation of the hybrid, which hindered the diffusion of CAS into the lumen. However, it is evident that the difference between the 2-step and 1-step method became smaller as the mixing time increased. One explanation for this is that CNFs originally adsorbed on HNTs were partly detached because of prolonged mixing, making both HNTs and CNFs available for adsorbing CAS. The different removal efficiencies obtained for the 2-step method without or with 30 min sedimentation support the statement that is important for both the

dye removal and turbidity reduction to allow the system to reach the equilibrium again after prolonged mixing. In conclusion, the sequential, 2-step method works best when HNTs are allowed to interact with the treated solution for a prolonged time, after which the pollutant-loaded particles can be rapidly aggregated by CNFs.

The optimized conditions for the removal of CAS (initial concentration 50 mg/L) by the 2–step method is summarized in Table 2. In addition to the reaction kinetics, the table contains the conclusions drawn from the previous sections regarding the optimum CNF dose (section 3.1, good turbidity reduction with 15 mg/g of CNFs) and pH (section 3.2, no interference in the analysis above pH>6.5).

Table 2. Optimized adsorption conditions for the removal of chrome azurol S by the sequential combination of halloysite nanotubes (HNTs) and cellulose nanofibrils (CNFs)

Step	Nanomaterial	Dose	Mixing Conditions	Note
1	HNTs	2 g/L	24 h, pH 7, 200 rpm	Used as received
2	CNFs	30 mg/L, 15 mg/g HNT	1–5 min, pH 7, 200 rpm	Added as a dilute suspension (0.2% w/w)

3.5 Characteristics of CNFs

CNFs had a cationic charge of ~1.0 meq/g in the pH range of 3–9, explaining the constant 20% CAS removal observed with pure CNFs at pH 6–8.5. The charge remained stable in aqueous solution for at least 17 weeks (Figure 4A). These findings are promising, because good stability

with respect to pH and over time is important when considering industrial-scale applications. At pH 10, the charge decreased to ~0.7 meq/g. This was likely caused by β-alkoxy fragmentation of the DAC backbone (bond between C-5 and O-5) in basic conditions [72], as has been previously noted [59,60]. Also, deprotonation of guanidinium ions is possible, although guanidine is a very strong base (pK_a 13.6) [73]. However, such highly basic conditions are not typically encountered in conventional municipal wastewater treatment plants.

The chemical modifications of cellulose were visible in the infrared spectra (Figure 4B). The spectrum of DAC presented a band at 1729 cm^{-1}, which is characteristic of an aldehyde carbonyl group (–CHO), whereas CDAC and CNFs exhibited two new bands at 1642 cm^{-1} and 1680 cm^{-1}, attributed respectively to N–H bond bending and C=N bond vibration [74,75]. The crystalline structure of cellulose remained intact during the chemical modifications and the mechanical disintegration, as the diffractograms showed typical cellulose I peaks (Figure 4C). Oxidation to DAC decreased the crystallinity index (CrI) of the cellulose pulp from 76% to 58%, as expected [76,77]. Cationization of DAC into CDAC in DES did not have any effect on the crystallinity (59%), while mechanical processing into CNFs decreased it slightly (48%). According to high-resolution TEM images, the CNF sample consisted of elongated fibrils approximately 5 nm or less in width, with alternating crystalline and disordered regions (Figure S10), as has been previously observed for bleached birch pulp (4.6 ± 1.1 nm, TEM analysis) [49].

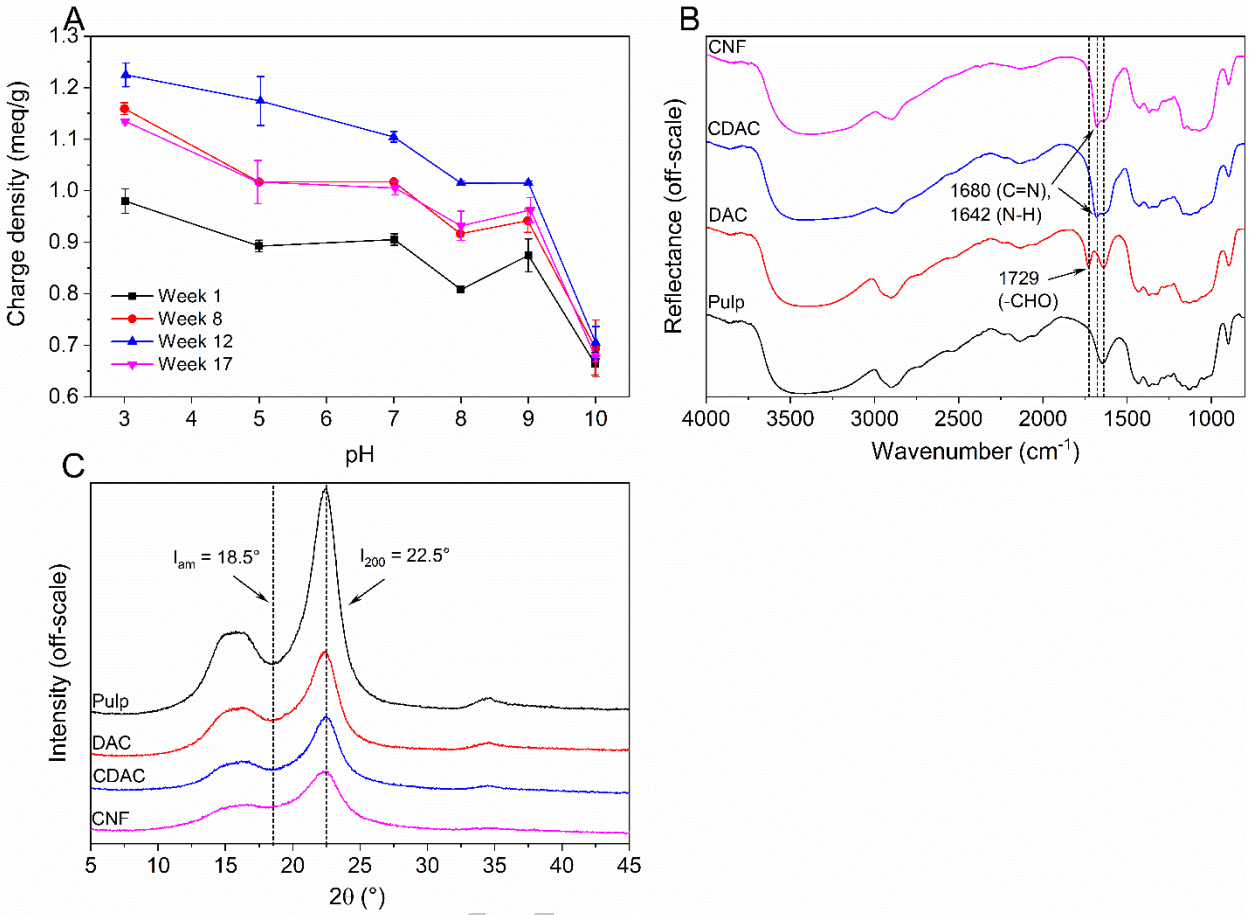

Figure 4. (A) The charge densities of cellulose nanofibrils as a function of pH. The data points are averages from three titrations and the error bars represent the sample standard deviation. (B) Diffuse reflectance spectra and (C) diffractograms of cellulose pulp, dialdehyde cellulose (DAC), cationized dialdehyde cellulose (CDAC), and cellulose nanofibrils (CNF).

3.6 Characteristics of clay minerals

The outer and inner diameters of HNTs measured from TEM images were ~30–80 nm and ~10–20 nm (Figure 5A), respectively, which matched the measured properties and manufacturer's specifications (Table S1). According to the laser diffractometry analysis (Figure 5B), the kaolin particles were <45 μm in diameter with a mean of 7 μm, which was also in line with the

manufacturer's specifications (Table S1). HNTs were rigid and tubular in morphology, whereas kaolin particles were layered, sharp-edged platelets (Figure 5C and D).

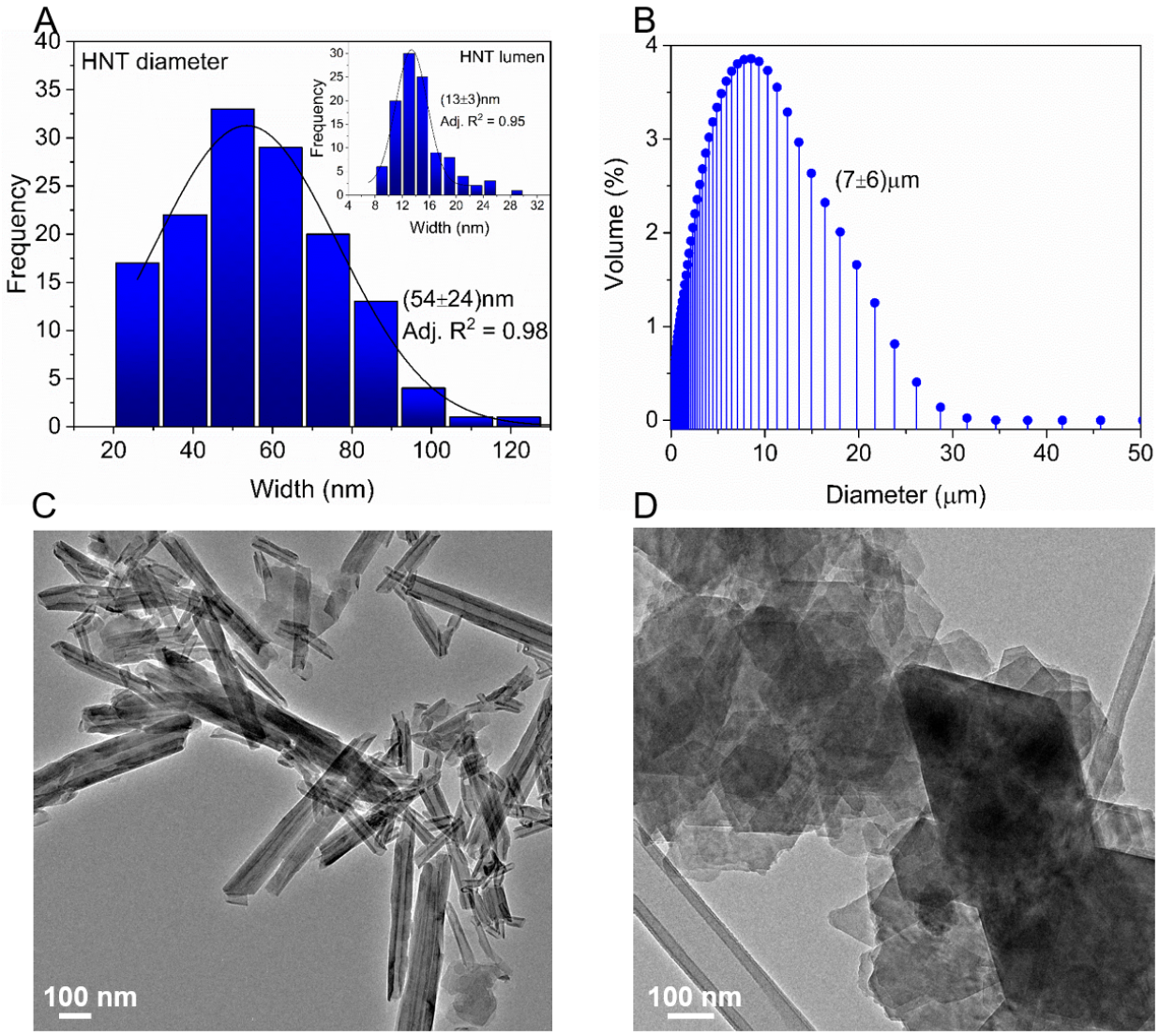

Figure 5. (A) Width distributions for halloysite nanotubes (inset: lumen width). Gaussian fitting (n >100) was used to evaluate the peak centers. (B) Diameter distribution for kaolin. TEM images of (C) halloysite nanotubes and (D) kaolin.

3.7 Characteristics of CAS-loaded HNT/kaolin–CNF aggregates

Cryo-SEM was utilized to image the aqueous CAS-loaded HNT/kaolin–CNF aggregates. Freeze-dried HNT–CNF aggregates formed continuous three-dimensional porous structures (Figure 6A1–A3) that resembled CNF sponges [78]. HNTs are capable of self-assembly and orienting themselves along the edge of a drying droplet (i.e., they exhibit the "coffee ring" effect), and this orientation is more pronounced for HNTs with high negative ζ-potential (e.g., because of the adsorption of anionic substances in the lumen) [79]. Therefore, it can be deduced that HNTs loaded with anionic CAS oriented themselves along the flexible CNF bundles during the sublimation process. Also, the shorter length of HNTs compared with that of CNFs probably facilitated this orientation. Interestingly, although the aggregates appear to consist mainly of CNFs (Figure 6A1–A3), the actual CNF:HNT ratio in this sample was 1:100 (CNFs 20 mg/L, HNTs 2 g/L). This again highlights the efficiency of CNFs in colloid removal and implies that the cost of the process can remain reasonable upon scaling, thanks to the lower consumption of the more expensive component (i.e., CNFs). Freeze-dried kaolin–CNF aggregates formed layered and less porous structures than HNT–CNF aggregates (Figure 6B1–B3). This is probably due to the different morphology and larger size of kaolin particles compared with HNTs. Based on the images, the faces of the kaolin platelets were covered with CNFs and connected to one another with CNF bundles (Figure 6B3).

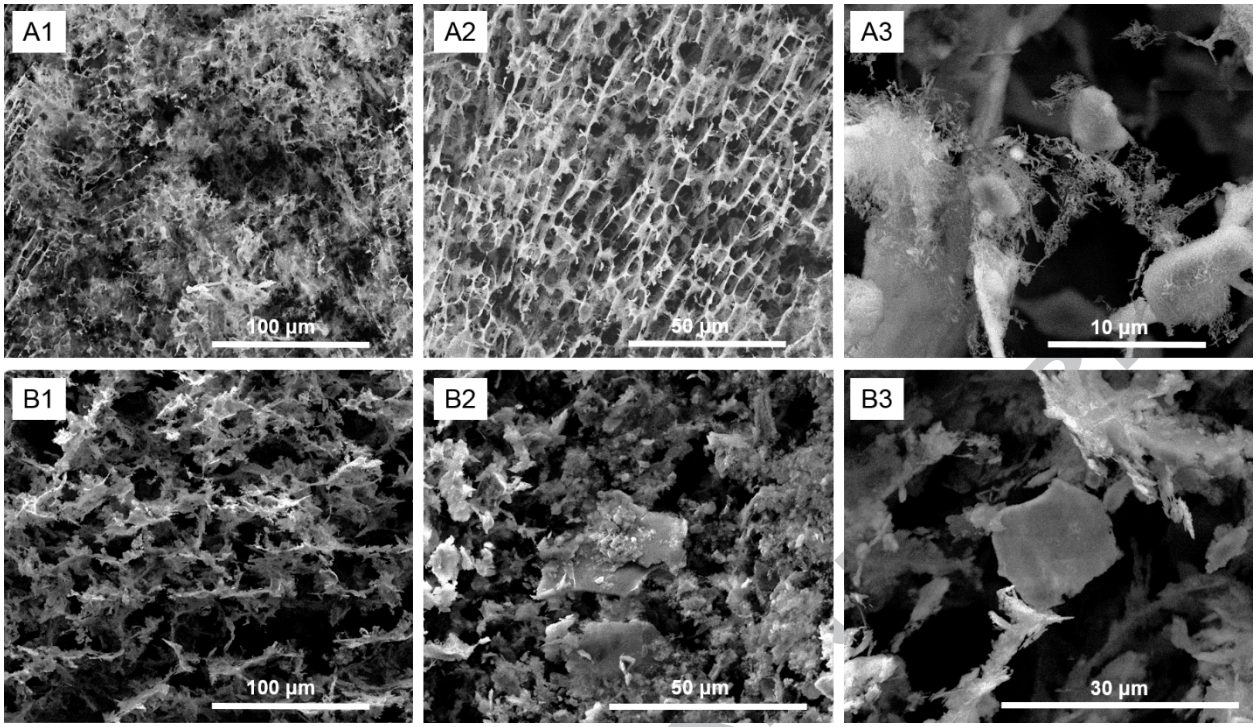

Figure 6. Cryo-SEM images of clay–cellulose nanofibrils–chrome azurol S aggregates with different magnifications. (A1–A3) Aggregates with halloysite nanotubes, scale bar 10–100 µm and (B1–B3) aggregates with kaolin, scale bar 30–100 µm.

Regarding the recyclability of the used adsorbents, one option could be the separation of the constituents forming aggregates and their reuse or disposal. However, the complete separation of CNFs from HNTs is expected to be laborious. In addition, the consequent purification process required to remove adsorbed CAS (e.g. washing) could damage the CNF structure and alter its properties, which could prevent its reuse in the process. Fortunately, CNFs are biodegradable which means that it could be decomposed. The purification of HNTs would be more straightforward involving e.g. washing with water [80] or with acids [14], after which they could be reused. Another more applicable and straightforward method would be a heat treatment. After burning away the organic constituents (CAS and CNFs), HNTs could be recycled back to the process. It should be taken into a consideration however, that washing with concentrated acids

[81] and heat treatments [82] can induce irreversible morphology changes in HNTs that can have an impact on their performance.

4 Conclusions

The sequential combination HNTs and CNFs resulted in significantly improved removal of anionic dye compared with using either of them alone. The size and morphology of the clay mineral had a clear impact on the outcome, as the nano-sized HNTs performed better than the micro-sized kaolin. The demonstrated concept is simple and requires no chemical pretreatments of the clay mineral (e.g., tube etching) or heavy energy usage (e.g., drying, vacuum). Moreover, both nanomaterials are abundantly available and can be processed sustainably (e.g., cellulose pulp obtained through DES treatment). The effective CNF dose for colloid removal was 10 mg/g, implying that the cost of the concept can be expected to remain reasonable upon scaling to industrial levels. In addition, the implementation of HNTs in existing wastewater treatment processes should be quite straightforward and require no extensive investments or alterations, because clay-based treatments (e.g., for enhanced sedimentation) are already used in some processes. However, the stability of the aggregates and the uptake of different pollutants into HNTs, as well as their release profiles, should be tested, preferably with low concentrations of pollutants (~µg/L level).

Acknowledgements

Ms. Eveliina Kuorikoski is acknowledged for her assistance in the laboratory experiments and Mr. Panpan Li is acknowledged for his advice in the preparation of CNFs. We would also like to thank Mr. Jarno Karvonen for performing the LS measurements, Mrs. Kaisu Ainassaari for

performing the BET analysis, Mr. Marcin Selent from the Center of Microscopy and Nanotechnology at the University of Oulu for performing the XRD measurements, and Mr. Jens Kling for performing the high-resolution TEM imaging of CNFs. Grateful thanks are also offered to KaMin LLC for providing us with a sample of the kaolin clay. TEM and SEM were performed at DTU Nanolab, the National Center for Nano Fabrication and Characterization at the Technical University of Denmark.

Funding: This work was supported by the Advanced Materials Doctoral Program of the University of Oulu Graduate School and the Bionanochemicals project of the Academy of Finland [grant number 298295].

Appendix A. Supplementary Material

Supplementary material associated with this article can be found, in the online version, at

References

[1] F. Bergaya, G. Lagaly, Chapter 1 General Introduction: Clays, Clay Minerals, and Clay Science, in: F. Bergaya, B.K.G. Theng, G. Lagaly (Eds.), Developments in Clay Science, Elsevier, 2006: pp. 1–18. doi:10.1016/S1572-4352(05)01001-9.

[2] E. Joussein, S. Petit, J. Churchman, B. Theng, D. Righi, B. Delvaux, Halloysite clay minerals — a review, Clay Minerals. 40 (2005) 383–426. doi:10.1180/0009855054040180.

[3] G. Lazzara, G. Cavallaro, A. Panchal, R. Fakhrullin, A. Stavitskaya, V. Vinokurov, Y. Lvov, An assembly of organic-inorganic composites using halloysite clay nanotubes, Current Opinion in Colloid & Interface Science. 35 (2018) 42–50. doi:10.1016/j.cocis.2018.01.002.

[4] L. Lisuzzo, G. Cavallaro, F. Parisi, S. Milioto, G. Lazzara, Colloidal stability of halloysite clay nanotubes, Ceramics International. (2018). doi:10.1016/j.ceramint.2018.07.289.

[5] B. Micó-Vicent, F.M. Martínez-Verdú, A. Novikov, A. Stavitskaya, V. Vinokurov, E. Rozhina, R. Fakhrullin, R. Yendluri, Y. Lvov, Stabilized Dye-Pigment Formulations with Platy and Tubular Nanoclays, Advanced Functional Materials. 28 (2018) 1703553. doi:10.1002/adfm.201703553.

[6] Y. Lee, G.-E. Jung, S.J. Cho, K.E. Geckeler, H. Fuchs, Cellular interactions of doxorubicin-loaded DNA-modified halloysite nanotubes, Nanoscale. 5 (2013) 8577. doi:10.1039/c3nr02665e.

[7] G.I. Fakhrullina, F.S. Akhatova, Y.M. Lvov, R.F. Fakhrullin, Toxicity of halloysite clay nanotubes in vivo: a Caenorhabditis elegans study, Environmental Science: Nano. 2 (2015) 54–59. doi:10.1039/C4EN00135D.
[8] G. Cavallaro, G. Lazzara, S. Milioto, F. Parisi, V. Evtugyn, E. Rozhina, R. Fakhrullin, Nanohydrogel Formation within the Halloysite Lumen for Triggered and Sustained Release, ACS Applied Materials & Interfaces. 10 (2018) 8265–8273. doi:10.1021/acsami.7b19361.
[9] V. Bertolino, G. Cavallaro, G. Lazzara, S. Milioto, F. Parisi, Biopolymer-Targeted Adsorption onto Halloysite Nanotubes in Aqueous Media, Langmuir. 33 (2017) 3317–3323. doi:10.1021/acs.langmuir.7b00600.
[10] M.-T. Viseras, C. Aguzzi, P. Cerezo, G. Cultrone, C. Viseras, Supramolecular structure of 5-aminosalycilic acid/halloysite composites, Journal of Microencapsulation. 26 (2009) 279–286. doi:10.1080/02652040802312499.
[11] M. Liu, R. Fakhrullin, A. Novikov, A. Panchal, Y. Lvov, Tubule Nanoclay-Organic Heterostructures for Biomedical Applications, Macromolecular Bioscience. (2018). doi:10.1002/mabi.201800419.
[12] E.A. Naumenko, I.D. Guryanov, R. Yendluri, Y.M. Lvov, R.F. Fakhrullin, Clay nanotube–biopolymer composite scaffolds for tissue engineering, Nanoscale. 8 (2016) 7257–7271. doi:10.1039/C6NR00641H.
[13] A. Panchal, G. Fakhrullina, R. Fakhrullin, Y. Lvov, Self-assembly of clay nanotubes on hair surface for medical and cosmetic formulations, Nanoscale. 10 (2018) 18205–18216. doi:10.1039/C8NR05949G.
[14] H. Chen, J. Zhao, J. Wu, H. Yan, Selective desorption characteristics of halloysite nanotubes for anionic azo dyes, RSC Advances. 4 (2014) 15389. doi:10.1039/c3ra47561a.
[15] P. Luo, Y. Zhao, B. Zhang, J. Liu, Y. Yang, J. Liu, Study on the adsorption of Neutral Red from aqueous solution onto halloysite nanotubes, Water Research. 44 (2010) 1489–1497. doi:10.1016/j.watres.2009.10.042.
[16] M. Zhao, P. Liu, Adsorption behavior of methylene blue on halloysite nanotubes, Microporous and Mesoporous Materials. 112 (2008) 419–424. doi:10.1016/j.micromeso.2007.10.018.
[17] Y. Dong, Z. Liu, L. Chen, Removal of Zn(II) from aqueous solution by natural halloysite nanotubes, Journal of Radioanalytical and Nuclear Chemistry. 292 (2012) 435–443. doi:10.1007/s10967-011-1425-z.
[18] G. Kiani, High removal capacity of silver ions from aqueous solution onto Halloysite nanotubes, Applied Clay Science. 90 (2014) 159–164. doi:10.1016/j.clay.2014.01.010.
[19] J. Li, F. Wen, L. Pan, Z. Liu, Y. Dong, Removal of radiocobalt ions from aqueous solutions by natural halloysite nanotubes, Journal of Radioanalytical and Nuclear Chemistry. 295 (2013) 431–438. doi:10.1007/s10967-012-1823-x.
[20] R. Cheng, H. Li, Z. Liu, C. Du, Halloysite Nanotubes as an Effective and Recyclable Adsorbent for Removal of Low-Concentration Antibiotics Ciprofloxacin, Minerals. 8 (2018) 387. doi:10.3390/min8090387.
[21] L. Ghezzi, A. Spepi, M. Agnolucci, C. Cristani, M. Giovannetti, M.R. Tiné, C. Duce, Kinetics of release and antibacterial activity of salicylic acid loaded into halloysite nanotubes, Applied Clay Science. 160 (2018) 88–94. doi:10.1016/j.clay.2017.11.041.
[22] I. Anastopoulos, A. Mittal, M. Usman, J. Mittal, G. Yu, A. Núñez-Delgado, M. Kornaros, A review on halloysite-based adsorbents to remove pollutants in water and wastewater, Journal of Molecular Liquids. 269 (2018) 855–868. doi:10.1016/j.molliq.2018.08.104.

[23] L. Yu, H. Wang, Y. Zhang, B. Zhang, J. Liu, Recent advances in halloysite nanotube derived composites for water treatment, Environmental Science: Nano. 3 (2016) 28–44. doi:10.1039/C5EN00149H.
[24] D. Tao, Y. Higaki, W. Ma, A. Takahara, Halloysite Nanotube/Polyelectrolyte Hybrids as Adsorbents for the Quick Removal of Dyes from Aqueous Solution, Chemistry Letters. 44 (2015) 1572–1574. doi:10.1246/cl.150727.
[25] S. Yang, P. Zong, J. Hu, G. Sheng, Q. Wang, X. Wang, Fabrication of β-cyclodextrin conjugated magnetic HNT/iron oxide composite for high-efficient decontamination of U(VI), Chemical Engineering Journal. 214 (2013) 376–385. doi:10.1016/j.cej.2012.10.030.
[26] Y. Xie, D. Qian, D. Wu, X. Ma, Magnetic halloysite nanotubes/iron oxide composites for the adsorption of dyes, Chemical Engineering Journal. 168 (2011) 959–963. doi:10.1016/j.cej.2011.02.031.
[27] X. Wan, Y. Zhan, Z. Long, G. Zeng, Y. He, Core@double-shell structured magnetic halloysite nanotube nano-hybrid as efficient recyclable adsorbent for methylene blue removal, Chemical Engineering Journal. 330 (2017) 491–504. doi:10.1016/j.cej.2017.07.178.
[28] L. Liu, Y. Wan, Y. Xie, R. Zhai, B. Zhang, J. Liu, The removal of dye from aqueous solution using alginate-halloysite nanotube beads, Chemical Engineering Journal. 187 (2012) 210–216. doi:10.1016/j.cej.2012.01.136.
[29] Q. Peng, M. Liu, J. Zheng, C. Zhou, Adsorption of dyes in aqueous solutions by chitosan–halloysite nanotubes composite hydrogel beads, Microporous and Mesoporous Materials. 201 (2015) 190–201. doi:10.1016/j.micromeso.2014.09.003.
[30] J. Kurczewska, M. Cegłowski, G. Schroeder, Alginate/PAMAM dendrimer – Halloysite beads for removal of cationic and anionic dyes, International Journal of Biological Macromolecules. 123 (2019) 398–408. doi:10.1016/j.ijbiomac.2018.11.119.
[31] G. Cavallaro, A. Gianguzza, G. Lazzara, S. Milioto, D. Piazzese, Alginate gel beads filled with halloysite nanotubes, Applied Clay Science. 72 (2013) 132–137. doi:10.1016/j.clay.2012.12.001.
[32] J. Maity, S.K. Ray, Chitosan based nano composite adsorbent—Synthesis, characterization and application for adsorption of binary mixtures of Pb(II) and Cd(II) from water, Carbohydrate Polymers. 182 (2018) 159–171. doi:10.1016/j.carbpol.2017.10.086.
[33] J. Ma, Y. He, G. Zeng, X. Yang, X. Chen, L. Zhou, L. Peng, A. Sengupta, High-flux PVDF membrane incorporated with β-cyclodextrin modified halloysite nanotubes for dye rejection and Cu (II) removal from water, Polymers for Advanced Technologies. 29 (2018) 2704–2714. doi:10.1002/pat.4356.
[34] R.S. Hebbar, A.M. Isloor, A.K. Zulhairun, Mohd. Sohaimi Abdullah, A.F. Ismail, Efficient treatment of hazardous reactive dye effluents through antifouling polyetherimide hollow fiber membrane embedded with functionalized halloysite nanotubes, Journal of the Taiwan Institute of Chemical Engineers. 72 (2017) 244–252. doi:10.1016/j.jtice.2017.01.022.
[35] R.S. Hebbar, A.M. Isloor, Inamuddin, Mohd.S. Abdullah, A.F. Ismail, A.M. Asiri, Fabrication of polyetherimide nanocomposite membrane with amine functionalised halloysite nanotubes for effective removal of cationic dye effluents, Journal of the Taiwan Institute of Chemical Engineers. 93 (2018) 42–53. doi:10.1016/j.jtice.2018.07.032.
[36] G. Zeng, Z. Ye, Y. He, X. Yang, J. Ma, H. Shi, Z. Feng, Application of dopamine-modified halloysite nanotubes/PVDF blend membranes for direct dyes removal from wastewater, Chemical Engineering Journal. 323 (2017) 572–583. doi:10.1016/j.cej.2017.04.131.

[37] G. Zeng, Y. He, Y. Zhan, L. Zhang, Y. Pan, C. Zhang, Z. Yu, Novel polyvinylidene fluoride nanofiltration membrane blended with functionalized halloysite nanotubes for dye and heavy metal ions removal, Journal of Hazardous Materials. 317 (2016) 60–72. doi:10.1016/j.jhazmat.2016.05.049.
[38] G. Rytwo, The Use of Clay-Polymer Nanocomposites in Wastewater Pretreatment, The Scientific World Journal. 2012 (2012) 1–7. doi:10.1100/2012/498503.
[39] G. Rytwo, R. Lavi, Y. Rytwo, H. Monchase, S. Dultz, T.N. König, Clarification of olive mill and winery wastewater by means of clay–polymer nanocomposites, Science of The Total Environment. 442 (2013) 134–142. doi:10.1016/j.scitotenv.2012.10.031.
[40] G. Cavallaro, G. Lazzara, S. Milioto, Exploiting the Colloidal Stability and Solubilization Ability of Clay Nanotubes/Ionic Surfactant Hybrid Nanomaterials, The Journal of Physical Chemistry C. 116 (2012) 21932–21938. doi:10.1021/jp307961q.
[41] B. Bolto, D. Dixon, R. Eldridge, S. King, Cationic polymer and clay or metal oxide combinations for natural organic matter removal, Water Research. 35 (2001) 2669–2676. doi:10.1016/S0043-1354(00)00552-2.
[42] M. Huerta-Fontela, M.T. Galceran, F. Ventura, Occurrence and removal of pharmaceuticals and hormones through drinking water treatment, Water Research. 45 (2011) 1432–1442. doi:10.1016/j.watres.2010.10.036.
[43] F. Rol, M.N. Belgacem, A. Gandini, J. Bras, Recent advances in surface-modified cellulose nanofibrils, Progress in Polymer Science. 88 (2019) 241–264. doi:10.1016/j.progpolymsci.2018.09.002.
[44] D. Wang, A critical review of cellulose-based nanomaterials for water purification in industrial processes, Cellulose. (2018). doi:10.1007/s10570-018-2143-2.
[45] T. Saito, Y. Nishiyama, J.-L. Putaux, M. Vignon, A. Isogai, Homogeneous Suspensions of Individualized Microfibrils from TEMPO-Catalyzed Oxidation of Native Cellulose, Biomacromolecules. 7 (2006) 1687–1691. doi:10.1021/bm060154s.
[46] T. Selkälä, J.A. Sirviö, G.S. Lorite, H. Liimatainen, Anionically stabilized cellulose nanofibrils through succinylation pretreatment in urea-lithium chloride deep eutectic solvent, ChemSusChem. 9 (2016) 3074–3083. doi:10.1002/cssc.201600903.
[47] P.R. Sharma, R. Joshi, S.K. Sharma, B.S. Hsiao, A Simple Approach to Prepare Carboxycellulose Nanofibers from Untreated Biomass, Biomacromolecules. 18 (2017) 2333–2342. doi:10.1021/acs.biomac.7b00544.
[48] H. Liimatainen, M. Visanko, J.A. Sirviö, O.E.O. Hormi, J. Niinimaki, Enhancement of the Nanofibrillation of Wood Cellulose through Sequential Periodate–Chlorite Oxidation, Biomacromolecules. 13 (2012) 1592–1597. doi:10.1021/bm300319m.
[49] P. Li, J.A. Sirviö, B. Asante, H. Liimatainen, Recyclable deep eutectic solvent for the production of cationic nanocelluloses, Carbohydrate Polymers. 199 (2018) 219–227. doi:10.1016/j.carbpol.2018.07.024.
[50] J. Sirviö, A. Honka, H. Liimatainen, J. Niinimäki, O. Hormi, Synthesis of highly cationic water-soluble cellulose derivative and its potential as novel biopolymeric flocculation agent, Carbohydrate Polymers. 86 (2011) 266–270. doi:10.1016/j.carbpol.2011.04.046.
[51] J.A. Sirviö, Cationization of lignocellulosic fibers with betaine in deep eutectic solvent: Facile route to charge stabilized cellulose and wood nanofibers, Carbohydrate Polymers. 198 (2018) 34–40. doi:10.1016/j.carbpol.2018.06.051.

[52] A. Olszewska, P. Eronen, L.-S. Johansson, J.-M. Malho, M. Ankerfors, T. Lindström, J. Ruokolainen, J. Laine, M. Österberg, The behaviour of cationic NanoFibrillar Cellulose in aqueous media, Cellulose. 18 (2011) 1213. doi:10.1007/s10570-011-9577-0.
[53] A. Chaker, S. Boufi, Cationic nanofibrillar cellulose with high antibacterial properties, Carbohydrate Polymers. 131 (2015) 224–232. doi:10.1016/j.carbpol.2015.06.003.
[54] A. Pei, N. Butchosa, L.A. Berglund, Q. Zhou, Surface quaternized cellulose nanofibrils with high water absorbency and adsorption capacity for anionic dyes, Soft Matter. 9 (2013) 2047–2055. doi:10.1039/C2SM27344F.
[55] T.T.T. Ho, T. Zimmermann, R. Hauert, W. Caseri, Preparation and characterization of cationic nanofibrillated cellulose from etherification and high-shear disintegration processes, Cellulose. 18 (2011) 1391–1406. doi:10.1007/s10570-011-9591-2.
[56] P. Zerzucha, K. Pytlakowska, K. Kocot, Spectroscopic and electric properties of C.I. Mordant Blue 29: a theoretical and experimental study, New Journal of Chemistry. 37 (2013) 2810. doi:10.1039/c3nj00505d.
[57] J. Sirvio, U. Hyvakko, H. Liimatainen, J. Niinimaki, O. Hormi, Periodate oxidation of cellulose at elevated temperatures using metal salts as cellulose activators, Carbohydrate Polymers. 83 (2011) 1293–1297. doi:10.1016/j.carbpol.2010.09.036.
[58] L. Segal, J.J. Creely, A.E. Martin, C.M. Conrad, An Empirical Method for Estimating the Degree of Crystallinity of Native Cellulose Using the X-Ray Diffractometer., Textile Research Journal. 29 (1959) 786–794. doi:https://doi.org/10.1177/004051755902901003.
[59] H. Liimatainen, J. Sirviö, O. Sundman, M. Visanko, O. Hormi, J. Niinimäki, Flocculation performance of a cationic biopolymer derived from a cellulosic source in mild aqueous solution, Bioresource Technology. 102 (2011) 9626–9632. doi:10.1016/j.biortech.2011.07.099.
[60] H. Liimatainen, T. Suopajärvi, J. Sirviö, O. Hormi, J. Niinimäki, Fabrication of cationic cellulosic nanofibrils through aqueous quaternization pretreatment and their use in colloid aggregation, Carbohydrate Polymers. 103 (2014) 187–192. doi:10.1016/j.carbpol.2013.12.042.
[61] T. Selkälä, T. Suopajärvi, J.A. Sirviö, T. Luukkonen, G.S. Lorite, S. Kalliola, M. Sillanpää, H. Liimatainen, Rapid uptake of pharmaceutical salbutamol from aqueous solutions with anionic cellulose nanofibrils: The importance of pH and colloidal stability in the interaction with ionizable pollutants, Chemical Engineering Journal. 350 (2018) 378–385. doi:10.1016/j.cej.2018.05.163.
[62] Mordant Blue 29 (Product number D0241), TCI Chemicals. (n.d.). https://www.tcichemicals.com/eshop/en/fi/commodity/D0241/ (accessed March 11, 2019).
[63] Y. Zhao, E. Abdullayev, A. Vasiliev, Y. Lvov, Halloysite nanotubule clay for efficient water purification, Journal of Colloid and Interface Science. 406 (2013) 121–129. doi:10.1016/j.jcis.2013.05.072.
[64] L. Besra, D.K. Sengupta, S.K. Roy, P. Ay, Flocculation and dewatering of kaolin suspensions in the presence of polyacrylamide and surfactants, International Journal of Mineral Processing. 66 (2002) 203–232. doi:10.1016/S0301-7516(02)00066-2.
[65] A.M. Palomino, J.C. Santamarina, Fabric map for kaolinite: effects of pH and ionic concentration on behavior, Clays and Clay Minerals. 53 (2005) 211–223. doi:10.1346/CCMN.2005.0530302.

[66] D. Tan, P. Yuan, F. Dong, H. He, S. Sun, Z. Liu, Selective loading of 5-fluorouracil in the interlayer space of methoxy-modified kaolinite for controlled release, Applied Clay Science. 159 (2018) 102–106. doi:10.1016/j.clay.2017.04.008.
[67] M. Ishiguro, L.K. Koopal, Surfactant adsorption to soil components and soils, Advances in Colloid and Interface Science. 231 (2016) 59–102. doi:10.1016/j.cis.2016.01.006.
[68] H. Sehaqui, U.P. de Larraya, P. Tingaut, T. Zimmermann, Humic acid adsorption onto cationic cellulose nanofibers for bioinspired removal of copper(II) and a positively charged dye, Soft Matter. 11 (2015) 5294–5300. doi:10.1039/C5SM00566C.
[69] J.H. Callahan, K.D. Cook, Mechanism of surfactant-induced changes in the visible spectrometry of metal-Chrome Azurol S complexes, Analytical Chemistry. 56 (1984) 1632–1640. doi:10.1021/ac00273a022.
[70] O.Y. Nadzhafova, S.V. Lagodzinskaya, V.V. Sukhan, Test Paper for the Determination of Aluminum in Solution, 56 (2001) 4.
[71] A.Yu. Shishov, A.V. Bulatov, A.L. Moskvin, L.N. Moskvin, Simultaneous cyclic-injection spectrophotometric determination of aluminum and iron in petroleum products, Journal of Analytical Chemistry. 69 (2014) 1159–1164. doi:10.1134/S1061934814120132.
[72] P. Calvini, G. Conio, M. Lorenzoni, E. Pedemonte, Viscometric determination of dialdehyde content in periodate oxycellulose. Part I. Methodology, Cellulose. 11 (2004) 99–107. doi:10.1023/B:CELL.0000014766.31671.8d.
[73] J. Clayden, N. Greeves, S. Warren, P. Wothers, Organic Chemistry, Oxford: Oxford University Press, 2001.
[74] J.A. Sirviö, A.-K. Anttila, A.M. Pirttilä, H. Liimatainen, I. Kilpeläinen, J. Niinimäki, O. Hormi, Cationic wood cellulose films with high strength and bacterial anti-adhesive properties, Cellulose. 21 (2014) 3573–3583. doi:10.1007/s10570-014-0351-y.
[75] Y. Zhang, J. Jiang, Y. Chen, Synthesis and antimicrobial activity of polymeric guanidine and biguanidine salts, Polymer. 40 (1999) 6189–6198. doi:10.1016/S0032-3861(98)00828-3.
[76] A.J. Varma, V.B. Chavan, A study of crystallinity changes in oxidised celluloses, Polymer Degradation and Stability. 49 (1995) 245–250. doi:10.1016/0141-3910(95)87006-7.
[77] J.A. Sirviö, A. Kolehmainen, M. Visanko, H. Liimatainen, J. Niinimäki, O.E.O. Hormi, Strong, Self-Standing Oxygen Barrier Films from Nanocelluloses Modified with Regioselective Oxidative Treatments, ACS Applied Materials & Interfaces. 6 (2014) 14384–14390. doi:10.1021/am503659j.
[78] O. Laitinen, T. Suopajärvi, M. Österberg, H. Liimatainen, Hydrophobic, Superabsorbing Aerogels from Choline Chloride-Based Deep Eutectic Solvent Pretreated and Silylated Cellulose Nanofibrils for Selective Oil Removal, ACS Applied Materials & Interfaces. 9 (2017) 25029–25037. doi:10.1021/acsami.7b06304.
[79] Y. Zhao, G. Cavallaro, Y. Lvov, Orientation of charged clay nanotubes in evaporating droplet meniscus, Journal of Colloid and Interface Science. 440 (2015) 68–77. doi:10.1016/j.jcis.2014.10.050.
[80] H. Chen, H. Yan, Z. Pei, J. Wu, R. Li, Y. Jin, J. Zhao, Trapping characteristic of halloysite lumen for methyl orange, Applied Surface Science. 347 (2015) 769–776. doi:10.1016/j.apsusc.2015.04.167.
[81] D. Garcia-Garcia, J.M. Ferri, L. Ripoll, M. Hidalgo, J. Lopez-Martinez, R. Balart, Characterization of selectively etched halloysite nanotubes by acid treatment, Applied Surface Science. 422 (2017) 616–625. doi:10.1016/j.apsusc.2017.06.104.

[82] S. Kadi, S. Lellou, K. Marouf-Khelifa, J. Schott, I. Gener-Batonneau, A. Khelifa, Preparation, characterisation and application of thermally treated Algerian halloysite, Microporous and Mesoporous Materials. 158 (2012) 47–54. doi:10.1016/j.micromeso.2012.03.014.

Highlights

- The stepwise addition of HNTs and CNFs efficiently removes anionic dye from water.
- Both HNTs and CNFs participate in the dye capture.
- CNFs also aggregate the dye-loaded colloidal clay particles.
- The size and morphology of the clay mineral determine the dye removal efficiency.